ORIGINAL ARTICLE

CrossMark

Study of the welding parameters effect on the tunnel void area during friction stir welding of 1060 aluminum alloy

Javad Rasti [1]

Abstract

Friction stir welding is a relatively novel solid state method which produces ultra fine-grained microstructure and promoted mechanical properties due to the severe plastic deformation induced during welding. These features, of course, would be obtained if the welding parameters have been justified so that the welding zone becomes free of any defect specially tunnel cavity. This defect was primarily caused by an insufficient heat input during welding. In this study, a mathematical model has been presented to estimate the heat input generation during welding pertaining to the frictional work dissipated between the tool/workpiece interface, and moreover, the heat produced by the mechanical stirring of the plastically deformed material around the pin. The aim was to correlate the heat input generation and the tunnel void area. Aluminum plates with commercial purity were used for experimental efforts. During friction stir welding, a thermal camera was utilized to measure the maximum temperature of the material. After welding, samples cut through the transverse direction and examined for the area of tunnel cavity, and the extent of thermo-mechanically affected zone, as well. Comparison among the tunnel cavity areas with the heat input generations showed that to eliminate the tunnel cavity, at least a minimum heat input of about 800 J mm^{-1} was required.

Keywords Friction stir welding · Heat input · Tunnel void · 1060 aluminum alloy

1 Introduction

When joining difficult to weld materials (such as Al, Ti, and Mg alloys but also Advanced High-Strength Steel), it is possible to refer to friction stir welding (FSW) technology (patented by TWI in 1991 [1]). FSW has recently received large attention from automotive and transportation [2], aeronautical [3], and petrochemical and power-plant industries [4].

Since 1991, the process has grown appreciably. Advances include the change of tool geometry (pin and shoulder design), tool materials, implementation procedure, and also the development of the process from an operational point of view, including stationary shoulder FSW [5], friction stir spot welding (FSSW) [6], bobbin FSW [7], reverse dual rotation FSW [8], and so on.

Pertaining to the tool geometry, several pin shapes, including simple cylindrical designs, tapered, and polygonal shapes (triangle, square, pentagon, hexagon) [9, 10] to complicated ones, such as threaded pins [11], Trivex™, Triflat™, triflute™, and quadflute™ pins [12, 13], have been introduced by researchers so far. Variety of tool materials were used for joining of different materials, as well. These materials include cold work steel 1.2080 (equivalent norms are D3, K100, SPK, X210cr12, SKD1), hot work steel 1.2344 (H13, SKD61), and high speed steel M2, M42, and W9 for joining of non-ferrous alloys especially aluminum alloys, and tungsten carbide, tungsten-rhenium alloy, and polycrystalline cubic boron nitride (PCBN) for welding of carbon steels [14]. The evolution, however, is not ended and further improvements are needed in this field.

FSW process is regarded to be an advanced welding technique because of material enhancement achieved in

✉ Javad Rasti
   rasti@qut.ac.ir; rastinik@gmail.com

[1]   Department of Mechanical Engineering, Qom University of Technology, Martyred Brigadier Khodakaram Blvd, Old Qom-Tehran road, P.O. Box: 1519-37195, Qom, Iran

the welding zone from the viewpoint of both micro-structural and mechanical aspects. However, these enhancements would be tangible when the weld zone becomes free of any flaw. Many defects have been reported to create in the welding zone during FSW. The main defects include voids, cracks, abnormal stirring, flow lines, large mass of flash due to the excess heat input, high volume of pleats around weld zone on surface, lack of penetration (LOP), "lazy S," and "kissing-bond" from survey of literatures [9, 15–17]. Voids are typically in the two forms: channel or groove-like cavity referring almost to the tunnel void and voids resulting from unsuitable mixing of material. Lazy S is a series of regularly black spaced curved lines occurring in the nugget zone, which originated from the oxide layer on the initial butt surface, which was then broken up, extruded, and deformed during FSW. Kissing-bond defect demonstrates a shingle lap pattern on the fracture surface, and it is likely caused when a cold deformed metal flows around the pin during a revolutionary pitch and comes into contact with the leaving advance-side surface behind the pin so that incomplete mixing is resulted. Among these defects, however, tunnel void is one of the most typical flaws in the stir zone. This defect is a very serious flaw, which adversely affects the tensile properties and elongation percentage greatly. Usually, the tunnel cavity results from the low rotational speed and the insufficient pressure [15].

The aim of this study was the consideration of extent of tunnel voids created in different welding conditions and how the welding parameters affect that. Since the heat generated in the welding zone includes the effects of all factors, and moreover, same as the most joining processes, heat input has the main roll to establish the qualified and sound weld, this factor was considered for correlation with the tunnel void area.

The analytical model for the heat generation given by Schmidt et al. is as follows [18]:

$$dQ = \omega \, dM = \omega \, r \, \tau \, dA \qquad (1)$$

where ω is the angular velocity and M is the torque exerted on the tool. This approach has been used by so many researchers [19–21] and found that a good agreement was obtained with the experimental results. The contact shear stress parameter τ in Eq. (1) can be written as a linear combination of full sliding ($\delta = 0$) and full sticking ($\delta = 1$) conditions as follows:

$$\tau = \delta \tau_y + (1-\delta)\mu P \qquad (2)$$

where τ_y is the shear yield strength, μ is the friction coefficient, and P is the normal pressure exerted on the work-piece by the tool. Gadakh et al. [22] developed an analytical model for heat generation for tapered cylindrical pin profile having flat shoulder in FSW

based on different assumptions in terms of contact conditions. Furthermore, Essa et al. [23] have presented an analytical model for the heat generation using eccentric cylindrical pin in FSW.

In the most analytical works published earlier, the heat generation was merely considered owing to contact condition of the work-piece/tool interface regarding the sliding or sticking terms. However, in this study, in addition to considering that component, the heat dissipated from the mechanical heating that arises from the viscous stirring of the deformed material around the pin in thermo-mechanically affected zone (TMAZ) has been taken into account. Eventually, by deriving the heat input equation and correlating that to the tunnel void area, the minimum heat input needed to create tunnel void-free welds was acquired.

2 Materials and method

2.1 Material and apparatus

The base material used in this study was 5-mm-thick commercially pure 1060 aluminum alloy sheet. Samples with length of 15 cm and width of 5 cm were cut from the raw sheet and then two sheets brought into contact firmly by clamping tools and special fixture on the T-slot table.

A friction stir welding machine with an AC motor coupled with an invertor for longitudinal movement and a hydraulic actuator for the vertical motion was employed in this study. A low-pressure indicator gauge (up to 10 bar) with accuracy of 1% was utilized to determine the downward force exerted on the welding face by the shoulder. Weldings were accomplished in different conditions including 500 and 1000 rpm for the rotational speed, 250, 500, and 650 mm/min for the welding traverse speed, and 6.9 and 13.8 MPa for the normal pressure. The tool shape was simple cylindrical shape comprised a pin with a diameter and height of 5 and 4.9 mm, respectively, and a shoulder with a diameter of 15 mm without any pattern or taper. Tilt angle could not set in this FSW machine, and therefore, its value was zero.

After performing each welding process, the samples were cut transversely and grinded. Final finishing was accomplished by Spark machine at very low current intensity to reveal voids more sharply. Then, weld section was examined for the existing and the extent of the tunnel cavity. The tunnel void area was calculated by ImageJ™ software. Since the tunnel void area had a statistical nature, in each sample, three sections were cut and the average tunnel void area was measured and reported. Of course, the more innovative methods

of measuring the size of tunnel cavity such as radiography, CT-Scan, or C-Scan ultrasonic tests might be employed for the better results. However, the accuracy of the employed method was adequately suitable for the current research.

A Fluke TiS75 thermal imaging camera was utilized during welding to record experimentally the maximum temperature experienced by the material for each condition. This camera had capability to measure temperatures in the range of − 20 to 550 °C. The uncertainty in these measurements was ± 1 pct (or approximately ± 6 °C). The thermal emissivity for the infrared data was calibrated by imaging an aluminum plate heated to 350 °C and adjusting the emissivity value until the recorded temperature of the camera matched the reference temperature. The appropriate thermal emissivity value was determined to be 0.235.

2.2 Model description

In the present work, a new heat input generation model has been proposed for the FSW process. A simple tool design with flat shoulder face and centric cylindrical pin was used in this study. Figure 1 shows this tool with three different modes of expected heat generations. The following underlying assumptions were considered for this analytical modeling:

1. Suppose that the plastically deformed material goes around the pin, in which the material rotational speed decreases linearly from the pin angular velocity at the vicinity of the pin face to the zero value at the distance δ from the pin face. The distance δ may resemble the thickness of thermo-mechanically affected zone (TMAZ) beyond the nugget region. Then, the following relation for the material angular velocity was considered:

Fig. 1 Tool shape with three different modes of heat generations

$$\omega_r = \omega_p\left(1-\frac{r-r_p}{\delta}\right); \omega = 2\pi N;$$

$$N_r = N_p\left(1-\frac{r-r_p}{\delta}\right) = A - Br; A = \frac{N_p}{\delta}(r_p+\delta), B = \frac{N_p}{\delta} \quad (3)$$

where ω_p, N_p, and r_p are the angular velocity (rad/s), the rotational speed (rev/s), and the pin radius, respectively. The heat generated in this zone was named as Q1 in Fig. 1.

2. The simple sliding condition was considered for the workpiece/tool contact faces. The heat generated in this manner was marked as Q2 in Fig. 1.

3. As the tool moves along the welding line, it compresses the material ahead of the pin and some energies dissipate. The resultant heat generation was called as Q3 in Fig. 1.

In the following, derivation of the different heat generation terms of Q1, Q2, and Q3 would be illustrated.

2.2.1 Heat generation due to the materials rotation around the pin

The general expression for the heat generation is as follows [18, 22]:

$$dQ = \omega \, dM = \omega \, r \, dF = \omega \, r \, (\tau \, dA + A \, d\tau) \quad (4)$$

where the angular velocity, ω, is a function of radial distance as Eq. (3) and $A = 2\pi r \, h_P$ (h_P is the pin height). By considering $= k_a e^{(T_a/T_{max})} N_r^{\alpha}$, which its derivation will be presented afterward, the below relationship was explored for the heat generation Q1.

$$Q_1 = 2^\alpha (2\pi)^{2+\alpha} h_P \, k_a \, e^{(T_a/T_{max})} \left[\frac{(r_P+\delta)^2}{1+\alpha} + \frac{2\delta^2}{3+\alpha} - \frac{3\delta(r_P+\delta)}{2+\alpha}\right].N_P^{1+\alpha} \quad (5)$$

Derivation of the shear stress equation For the shear stress τ, the following relationship was proposed:

$$\tau = k_a e^{(T_a/T_{max})}\left(k_b + k_c\frac{du}{dr}\right)^\alpha \quad (6)$$

where k_a, k_b, k_c, α, and T_a are the constants, and T_{max} is the maximum (peak) temperature experienced by the material during welding process, and $u = r\omega$ is the linear velocity. This equation resembles the form of constitutive equation as below:

$$\sigma_y = A \, Z^\alpha = A \, e^{\left(\frac{\alpha Q}{RT}\right)} \dot{\varepsilon}^\alpha \quad (7)$$

where Z is the Zener-Hollomon parameter and $\sigma_y = \sqrt{3} \, \tau_y$ (Von-mises criterion). Comparing these two later equations reveals that $k_a = A/\sqrt{3}$, $T_a = \alpha Q/R$ and $\dot{\varepsilon} = k_b + k_c\frac{du}{dr}$.

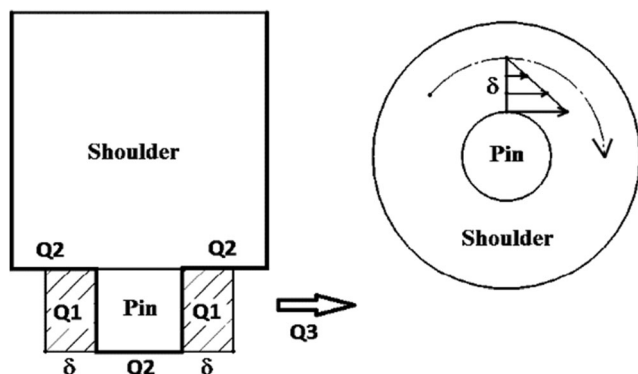A type of constitutive equation for 1060 aluminum alloy has been presented by Li et al. [24]. Stress-Strain rate
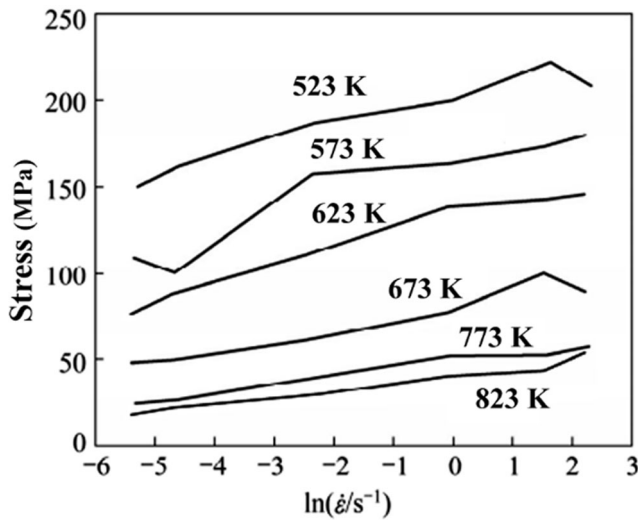
Fig. 2 Flow stress vs. ln$\dot{\varepsilon}$ curves of pure 1060 aluminum alloy at different temperatures [24]

curves withdrawn from their work are seen in Fig. 2. Using these curves and some regressions, the constants of Eq. (6) could be obtained as $\alpha = 0.23$, $T_a = 700$ K, and $K_a = 8.26$ MPa. On the other hand, the relation for the strain rate $\dot{\varepsilon} = k_b + k_c \frac{du}{dr}$ has not yet been determined. Putting $u = r\omega$ and using Eq. (3) results that $du/dr = A - 2Br$. Putting constants k_b and k_c to be $0.25A$ and 0.25, respectively, leads to $\dot{\varepsilon} = 0.5(A - Br) = 0.5N_r$. Whereas the rotational speed was 8.3 and 16.7 rev/s in the current study (i.e., 500 and 1000 rpm), so the strain rate became about 4–8 s^{-1} adjacent to the pin (ln($\dot{\varepsilon}$)$\cong$1.4−2). This approach is at good coincidence with the estimation presented by Husain et al. [25]. Therefore, the shear stress equation could be written as follows:

$$\tau = 7.04 \times e^{(700/T_{max})} N_r^{0.23} \tag{8}$$

Material maximum temperature (T_{max}) Arbegast and Hartley [26] demonstrated that a general relationship between peak temperature and FSW parameters can be explained as follows:

$$\frac{T_{max}}{T_m} = K \left(\frac{\omega^2}{\vartheta} \right)^{\beta} \tag{9}$$

where T_m is the melting point or solidus temperature of the alloy (°C), ω is the tool rotational speed, ϑ is the traverse speed, and the coefficient K and the exponent β are determined experimentally. These constants can be extracted for the different aluminum alloys based on the maximum temperature obtained experimentally from the different methods such as embedding thermocouples in the tool or the work piece, thermal cameras, correlation with the microstructure, simulation models, and temperature measurement methods based on ultrasound and neutron source. The above equation could be extracted for some aluminum alloys from survey of literature [27] in which results are seen in Table 1. Thermal properties of those alloys along with 1060 aluminum alloy are also presented in Table 2.

Based on the results of Tables 1 and 2, this is possible to make correlation between constants K and β with the alloy thermal diffusivity (α) and its solidus temperature. Figure 3 shows the variation of these constants (K and β) versus $\alpha/T_m \times 10^{-5}$. The fitted trend lines could be extrapolated to α/T_m of AA1060 aluminum alloy to determine approximately related parameters K and β for this alloy. In doing so, the following approach was considered for the maximum temperature:

$$\frac{T_{max}}{T_m} = 0.125 \times \left(\frac{\omega^2}{\vartheta} \right)^{0.12} \tag{10}$$

Table 1 Maximum temperatures and relevant fitted equations for some aluminum alloys

Alloy	Tool geometry			Welding parameters			Measured max. T (°C)	$\frac{\omega^2}{\vartheta} \times 10^3$	Solidus temp. (°C)	Fitted equation for $\frac{T_{max}}{T_m}$
	ro (mm)	ri (mm)	h (mm)	ω (rpm)	ϑ (mm/s)	F (kN)				
AA7108-T79	7.5	2.5	6	1500	5	7	375	450	475	$1.83 \times 10^{-3} \times \left(\frac{\omega^2}{\vartheta} \right)^{0.465}$
					8	7	290	281.2		$R^2 = 0.9877$
					12	7	250	187.5		
AA6082-T6	7.5	2.5	6	1500	5	7	321	450	606	$12.6 \times 10^{-3} \times \left(\frac{\omega^2}{\vartheta} \right)^{0.287}$
					8	7	275	281.2		$R^2 = 0.9912$
					12	7	250	187.5		
AA7050-T7451	9.5	3.2	6.4	490	1.4	20	220	171.5	488	$47.1 \times 10^{-3} \times \left(\frac{\omega^2}{\vartheta} \right)^{0.184}$
				700	1	13	260	490		$R^2 = 0.8644$
					1.9	16	220	257.9		
					2.6	18	216	188.5		

From [27]

Table 2 Thermal properties of aluminum alloys mentioned in Table 1

Alloy	ρ (kg/m^3)	C_P (J/kg/K)	K (W/m/K)	$\alpha \times 10^{-5}$	T_m (°C)
AA7108-T79	2780	960	140	5.2	475
AA6082-T6	2700	889	170	7.1	606
AA7050-T7451	2830	860	157	6.5	488
AA1060	2700	900	230	9.5	649

where ω is the rotational speed in RPM, ϑ is the traverse speed in mm/s, and T_{max} and T_m are the maximum and solidus temperature, respectively, in °C.

2.2.2 Heat generation from the workpiece/tool contact faces

The heat generated from the friction condition that existed between the tool and workpiece was formulated as follows:

$$Q_2 = (2\pi)^2 \mu P \left[\int_{r_P}^{r_P+\delta} r^2 \Delta N \, dr + \int_{r_P+\delta}^{r_{Sh}} r^2 N_P \, dr + \int_0^{r_P} r^2 N_P \, dr \right]$$

$$Q_2 = \frac{\pi^2}{3} \mu P N_P \left[4 \, r_{Sh}^3 - 6\delta r_P^2 - 4r_P\delta^2 - \delta^3 \right] \quad (11)$$

where μ is the friction coefficient, P is the normal pressure, and r_{Sh} is the shoulder radius.

2.2.3 Heat generation from the tool movement along the weld bead

As the tool moves along the welding line, it compresses and forces material to yield ahead of the pin. With resembling this situation to the pressured vessel condition, the following relation for the heat generation was attained in this mode:

$$Q_3 = 2 \, r_P \, h_P \, S_y \, V \quad (12)$$

where S_y is the flow stress of the material and V is the traverse speed.
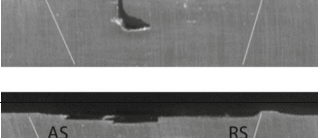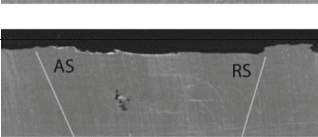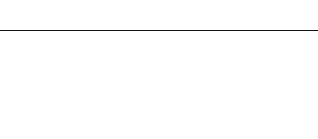
3 Results and discussion

Table 3 shows the cross-section of friction stir weldments in different welding conditions. The tunnel cavity areas calculated using ImageJ software were presented as well.

Figure 4 illustrates the void areas at different FSW conditions mentioned in Table 3. As can be seen, the largest tunnel cavity has been made at the rotational speed of 500 rpm and the normal pressure of 6.9 MPa. With increasing the normal pressure to 13.8 MPa and rotational speed to 1000 rpm, the tunnel cavity has become smaller in size. In each combination of pressure and rotational speed, raising the traverse speed causes the cavity to become larger in size. These results were all in accordance with the results presented by Kim et al. [15] and Zhang et al. [17]. This figure also shows that the influence of rotational speed is much greater than the normal pressure in terms of void diminishing.

Furthermore, it is interesting to notice to the tunnel void shape. As seen in macrographs presented in Table 3, some voids are "L" shape cross section whereas, the other voids have more circular cross section. This can be demonstrated by knowing the nature of tunnel void formation. Indeed, the tunnel cavity is formed when the velocity of the material in the longitudinal direction of the weld exceeds the material rotation around the pin. In other words, the forging force is not enough to drive the material from the retreating side to the advancing side behind the pin. As material experiences higher temperature beneath the shoulder, the

Fig. 3 Variation of constants K and β versus α/T_m in different aluminum alloys

Table 3 The calculated tunnel cavity areas in different conditions of FSW

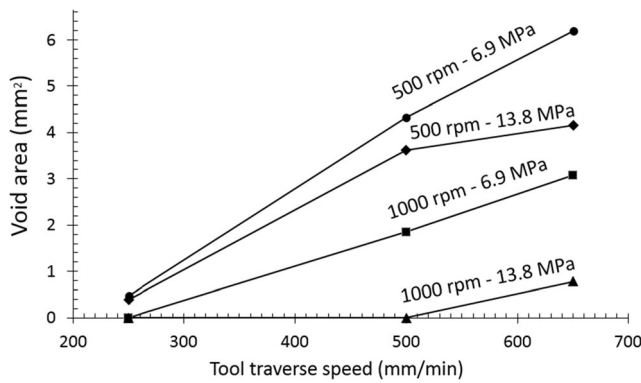| Test No.	Rotational speed (rpm)	Traverse speed (mm/min)	Normal pressure (MPa)	Cross section macrograph	Tunnel cavity area (mm²)
1	500	250	6.9		0.457
2	500	500	6.9		4.325
3	500	650	6.9		6.203
4	500	250	13.8		0.387
5	500	500	13.8		3.625
6	500	650	13.8		4.15
7	1000	250	6.9		0
8	1000	500	6.9		1.85
9	1000	650	6.9		3.075
10	1000	250	13.8		0
11	1000	500	13.8		0
12	1000	650	13.8		0.78

Fig. 4 Tunnel void areas at different FSW conditions

sticking condition is provided and the rotation of the material is done well and no cavity is created. By increasing the distance from the shoulder face, the rotational speed of the material reduces, thereby leading to cavity creation. If these cavities begin to create from the bottom half of the pin, they will eventually form "L" shape cavity. By increasing the tool rotation speed and the normal pressure, the cavity transfers from the pin body to the pin tip, leaving a more circular voids in shape.

Referring to the model presented in the previous section, we can calculate heat generation terms of Q1, Q2, and Q3. Consequently, heat input may be obtained from the following equation:

$$HI_i = \eta Q_i / \vartheta \qquad (13)$$

where η is the heat efficiency (≈ 0.9) and ϑ is the traverse speed.

To calculate heat input terms, however, it is preliminarily necessary to determine the distance δ and the peak temperature T_{max}. As above-mentioned, the distance δ can be candidate to the TMAZ extent. By this resembling, macroscopic investigations were done on the welding cross sections at various welding conditions. Figure 5 shows the macrostructure of sample no. 8 (1000 rpm, 500 mm/min, and 6.9 MPa) and the relevant regions. The extent of TMAZ region, hereafter called the distance δ, was calculated in the mid-thickness of weld zone.

The peak temperature T_{max} may be calculated according to Eq. (10). To validate this equation, the thermal
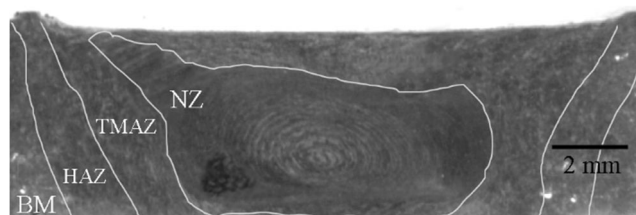

Fig. 5 Macrostructure of sample no. 8 and the relevant regions

camera was utilized. Figure 6 shows the maximum temperature measured in different samples (ID No. 1 to 12 ref. to Table 3) using thermal camera against Eq. (10). As can be seen, the trends are at good coincidence. Therefore, based on the maximum temperature measured by the thermal camera, the relation of Eq. (10) could be modified as below:

$$T_{max} = 0.065 \times \left(\frac{\omega^2}{\vartheta} \right)^{0.15} P^{0.14} T_m \qquad (14)$$

where ω is the rotational speed in RPM, ϑ is the traverse speed in mm/s, P is the normal pressure in MPa, and T_{max} and T_m are the maximum and solidus temperatures, respectively, in °C.

All the parameters obtained experimentally or via the modeling have been presented in Table 4.

As expected, the heat input generation from the tool traverse along the welding line (HI$_3$) is low comparatively and may be ignored. Figure 7 shows the variation of HI$_1$ and HI$_2$ heat inputs at different conditions of FSW. As seen, the HI$_1$ heat input (arises from the rotational stirring of the material around the pin) has low dependency to the normal pressure compared to the main rotational speed impact. On the other hand, both the normal pressure and the rotational speed have nearly the same effects on the HI$_2$ heat input (frictional term of the heat generation).

The effect of normal pressure on the HI$_1$ heat input is irrationally confusing. It is expected that with the higher normal pressure, the more HI$_1$ heat input is concluded (just like as HI$_2$), whereas contrarily, the inverse effect was attained. This repugnance can be illustrated as follows: As the normal pressure goes up, the maximum temperature of the material increases, thereby the distance δ (TMAZ extent) grows as well. These sequential events, which may reduce the strain rate in the TMAZ region, along with the increased maximum temperature, cause the lower shear stress which leads to the lower HI$_1$ heat input, as well. Total heat input obtained in the current study had good coincidence with the results presented through the literatures [21, 23].

A cavity or groove-like defect was primarily caused by an insufficient heat input during the FSW process [15]. Therefore, this is worthy to consider relation between the tunnel cavity area and the total heat input of the welding process. This is shown in Fig. 8. As seen in this figure, if the total heat input is greater than about 800 J/mm, the tunnel void diminishes and leads to making sound weld in the macroscopic scale. Of course, further research is needed to consider other defects in the microscopic scale.

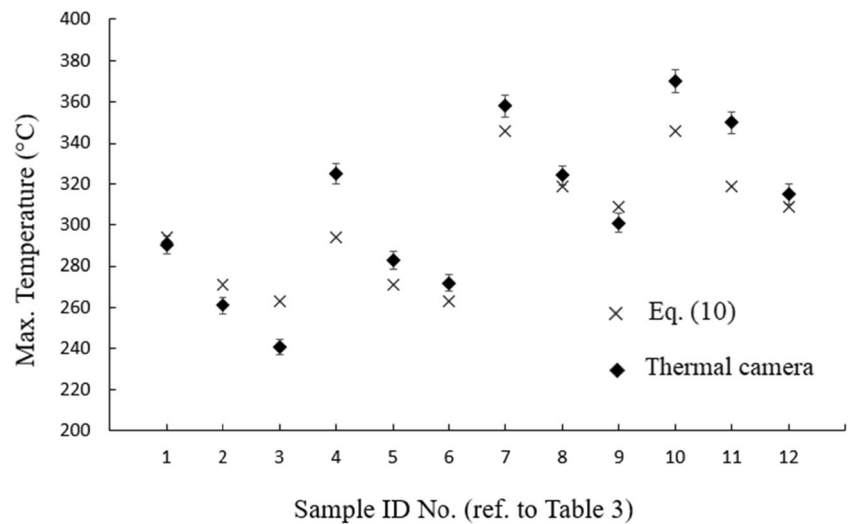**Fig. 6** Maximum temperature measured in the different samples using the thermal camera against Eq. (10)

Table 4 Different parameters obtained experimentally or based on the presented model

Test no.	ω (rpm)	ν (mm/min)	P (MPa)	HI_1 (J/mm)	HI_2 (J/mm)	HI_3 (J/mm)	HI_{total} (J/mm)	T_{max} (°C)	δ (mm)	τ (MPa)	T.C.A (mm²)
1	500	250	6.9	531	180	3	718	288	1.47	39.9	0.457
2	500	500	6.9	284	90	4	372	260	1.45	42.7	4.325
3	500	650	6.9	223	69	4	290	250	1.41	43.8	6.203
4	500	250	13.8	505	360	3	868	317	1.63	37.5	0.387
5	500	500	13.8	268	180	3	445	286	1.51	40.1	3.625
6	500	650	13.8	211	138	3	346	275	1.48	41.1	4.15
7	1000	250	6.9	1112	358	3	1375	355	1.72	41.0	0
8	1000	500	6.9	590	179	3	705	320	1.63	43.8	1.85
9	1000	650	6.9	467	138	3	548	307	1.67	44.9	3.075
10	1000	250	13.8	1057	713	3	1685	391	1.85	38.6	0
11	1000	500	13.8	563	357	3	859	352	1.82	41.2	0
12	1000	650	13.8	442	275	3	666	338	1.77	42.2	0.78

Fig. 7 Comparison of the HI_1 and HI_2 heat inputs in different conditions of FSW
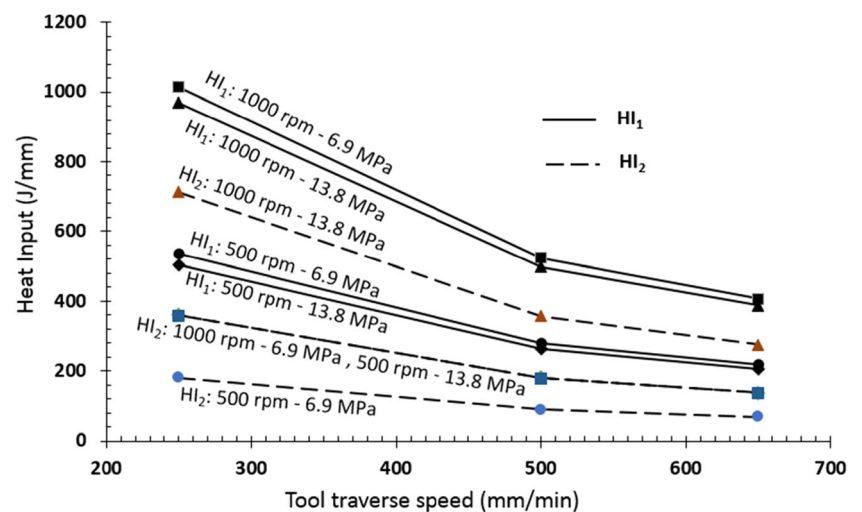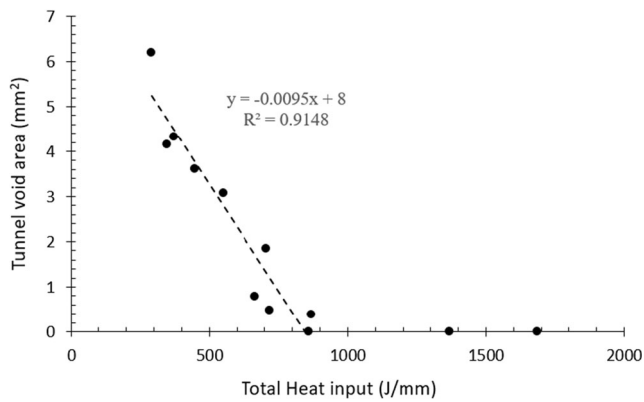
Fig. 8 Tunnel void area vs. heat input generated during welding

Finally, by some regressions, following relationship was explored among the total heat input data versus the variable parameters used in this study:

$$HI_t = 217.4 \, \omega^{0.96} \, V^{-0.963} P^{0.28} \tag{15}$$

where ω is the rotational speed in rpm, V is the traverse speed in mm/min, and P is the normal pressure in MPa.

By this simplification and by regarding the minimum heat input of 800 J/mm, the following relationship was suggested for the minimum rotational speed required to create tunnel void-free welds.

$$\omega_{min} = 3.89 \times V \times P^{-0.29} \tag{16}$$

In each FSW process, the same relationship may be explored for any specific defect in different alloys.

4 Conclusions

In this study, a mathematical model for the heat input generation during friction stir welding of 1060 aluminum alloy was presented. By comparison of the model results with the tunnel cavity areas measured experimentally, the following conclusions could be attained:

1. For elimination of the tunnel void in the friction stir welding of 1060 commercially pure aluminum, at least a measure of heat input about 800 J/mm is needed.
2. By regarding the minimum heat input generation suggested to create the tunnel void-free welds, a practical relation for the minimum tool rotational speed was presented in terms of the welding velocity and the normal pressure.

References

1. Thomas WM, Nicolas ED, Needham JC, Murch MG, Templesmith P, Dawes CJ (1991) Int Patent Application No PCT/GB92/02203
2. Kawasaki T, Makino T, Todori S, Takai H, Ezumi M, Inada Y (2000) Application of friction stir welding to the manufacturing of next generation A-train type rolling stock. Proceedings of 2nd International Symposium on Friction Stir Welding Gothenburg Sweden
3. Lohwasser D (2000) Application of friction stir welding for aircraft industry, Proceedings of 2nd Int Symp on FSW Gothenburg Sweden
4. Zucchi F, Trabanelli G, Grassi V (2001) Pitting and stress corrosion cracking resistance of friction stir welded AA 5083. Mater Corros 52:853–859
5. Wu H, Chen YC, Strong D, Prangnell P (2015) Stationary shoulder FSW for joining high strength aluminum alloys. J Mater Process Technol 221:187–196
6. Paidar M, Khodabandeh A, Lali Sarab M, Taheri M (2015) Effect of welding parameters (plunge depths of shoulder, pin geometry, and tool rotational speed) on the failure mode and stir zone characteristics of friction stir spot welded aluminum 2024-T3 sheets. J Mech Sci Technol 29(11):4639–4644
7. Thomas WM, Wiesner CS, Marks DJ, Staines DG (2009) Conventional and bobbin friction stir welding of 12% chromium alloy steel using composite refractory tool materials. Sci Technol Weld Join 14(3):247–253
8. Li JQ, Liu HJ (2013) Characteristics of the reverse dual-rotation friction stir welding conducted on 2219-T6 aluminum alloy. Mater Des 45:148–154
9. Kush PM, Vishvesh JB (2016) Effects of tool pin design on formation of defects in dissimilar friction stir welding. Procedia Technol 23:513–518
10. Mehta M, Reddy GM, Rao AV, De A (2015) Numerical modeling of friction stir welding using the tools with polygonal pins. Defence Technol 11:229–236
11. Radisavljevic IZ, Zivkovic AB, Grabulov VK, Radovic NA (2015) Influence of pin geometry on mechanical and structural properties of butt friction stir welded 2024-T351 aluminum alloy. Hem Ind 69(3):323–330. https://doi.org/10.2298/HEMIND131206020R
12. Su H, Wu CS, Bachmann M, Rethmeier M (2015) Numerical modeling for the effect of pin profiles on thermal and material flow characteristics in friction stir welding. Mater Des 77:114–125
13. Colegrove PA, Shercliff HR (2004) Two-dimensional CFD modelling of flow round profiled FSW tooling. Sci Technol Weld Join 9(6):483–492
14. Bozkurt Y, Boumerzoug Z (2017) Tool material effect on the friction stir butt welding of AA2124-T4 alloy matrix MMC. J Mater Res Technol https://doi.org/10.1016/j.jmrt.2017.04.001. Accessed 5 May 2017, Tool material effect on the friction stir butt welding of AA2124-T4 Alloy Matrix MMC
15. Kim YG, Fujii H, Tsumura T, Komazaki T, Nakata K (2006) Three defect types in friction stir welding of aluminum die casting alloy. Mater Sci Eng A 415:250–254
16. Chen HB, Yan K, Lin T, Chen SB, Jiang CY, Zhao Y (2006) The investigation of typical welding defects for 5456 aluminum alloy friction stir welds. Mater Sci Eng A 433:64–69
17. Zhang H, Lin SB, Wu L, Feng JC, Ma SL (2006) Defects formation procedure and mathematic model for defect free friction stir welding of magnesium alloy. Mater Des 27:805–809
18. Schmidt H, Hattel J, Wert J (2004) An analytical model for the heat generation in friction stir welding. Model Simul Mater Sci Eng 12:143–157

19. Khandkar MZH, Khan JA, Reynolds AP (2003) Prediction to temperature distribution and thermal history during friction stir welding: input torque based model. Sci Technol Weld J 8:165–174

20. Hamilton C, Dymek S, Sommers A (2008) A thermal model of friction stir welding in aluminum alloys. Int J Mach Tools Manuf 48:1120–1130

21. Arora A, Nandan R, Reynolds AP, DebRoy T (2009) Torque, power requirement and stir zone geometry in friction stir welding through modeling and experiments. Scr Mater 60:13–16

22. Gadakh VS, Kumar AK (2013) Heat generation model for taper cylindrical pin profile in FSW. Mater Res Technol J 2(4):370–375

23. Essa ARS, Ahmed MMZ, Mohamed AYA, El-Nikhaily AE (2016) An analytical model of heat generation for eccentric cylindrical pin in friction stir welding. J Mater Res Technol 5(3):234–240

24. Li P, Li F, Cao J, Ma X, Li J (2016) Constitutive equations of 1060 pure aluminum based on modified double multiple nonlinear regression model. Trans Nonferrous Met Soc China 26: 1079−1095

25. Husain MM, Sarkar R, Pal TK, Prabhu N, Ghosh M (2015) Friction stir welding of steel: heat input, microstructure, and mechanical property co-relation. J of Materials Engineering and Performance 24(9):3673–3683

26. Arbegast WJ, Hartley PJ (1998) Friction stir weld technology development at Lockheed Martin Michoud space systems—an overview. In Proceedings of the Fifth International Conference on Trends in Welding Research, Pine Mountain, GA, USA, 1–5 June, p 541

27. Hamilton C, Dymek S, Sommers A (2010) Characteristic temperature curves for aluminum alloys during friction stir welding. Weld J 89